

Selective reductive cleavage of C–O bond in lignin model compounds over nitrogen-doped carbon-supported iron catalysts

Jiang Li^{a,*}, Hui Sun^a, Jia-xing Liu^a, Jun-jie Zhang^a, Zhen-xing Li^a, Yao Fu^b

^a State Key Laboratory of Heavy Oil Processing, Institute of New Energy, China University of Petroleum (Beijing), Beijing, 102249, China

^b Anhui Province Key Laboratory of Biomass Clean Energy, Department of Chemistry, University of Science and Technology of China, Hefei, 230026, China

ARTICLE INFO

Keywords:

Biomass conversion
Lignin
C–O bond cleavage
Heterogeneous catalysis
Iron

ABSTRACT

Lignin has recently attracted much attention as a promising resource to produce fuels and aromatic chemicals. The selective cleavage of C–O bond while preserving the aromatic nature has become one of the major challenges in the catalytic valorization of lignin to aromatic chemicals. In this work, we report that the selective reductive cleavage of C–O bond in lignin model compounds can be successfully achieved through heterogeneous iron catalysis. The hydrogenolysis of α -O-4 model linkage shows that the iron catalyst prepared by the simultaneous pyrolysis of iron acetate and 1,10-phenanthroline on activated carbon at 800 °C is the most active iron catalyst, affording phenol and toluene with yields of 95% and 90%, respectively. This aromatics selectivity is found to be much higher than that obtained over noble metal catalysts. The presence of N...Fe species as the active center of heterogeneous iron catalyst was confirmed by various technologies especially XPS and H₂-TPR. For the β -O-4 model linkage, the vicinal –OH group was essential for the iron-catalyzed hydrogenolysis of ether linkage. The oxidation of the α -carbon in the β -O-4 model compounds can significantly decrease the bond dissociation energy of ether linkage, giving depolymerization products in moderate to excellent yields.

1. Introduction

The rapid decline of fossil reserves and increasing demand for energy have prompted researchers to utilize alternative sustainable resources, such as biomass, for the production of fuels and chemicals [1,2]. As one of the three main components of lignocellulosic biomass, lignin has been regarded as a promising resource to produce valuable aromatic compounds [3]. It is composed of methoxy-substituted phenyl and phenolic subunits linked together through C–O bonds of α - and β -arylalkyl ethers. Currently, selective cleavage of C–O bond while preserving its aromatic nature has become one of the major challenges in the catalytic valorization of lignin to aromatic chemicals.

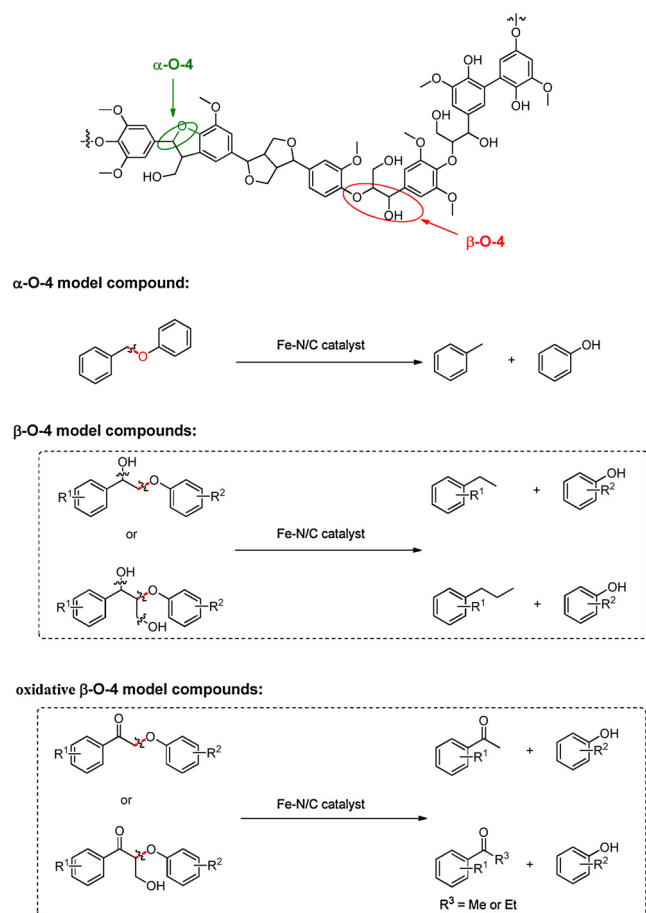
Well-defined molecular catalysts were first used for the selective cleavage of lignin-derived aryl ether linkages. Hartwig and co-workers reported an effective nickel carbene complex for the hydrogenolysis of aromatic C–O bonds in alkyl aryl and diaryl ethers [4]. Some other molecular catalysts based on Ru [5–7], V [8,9], Fe [10], Ir [11,12] and Re [13] complexes have also been reported for the selective C–O bond cleavage. Although the molecular catalysts can be easily accessible to react with individual ether linkage, they also suffer from sensible to water, which is costly to remove during biomass conversion. Hence, various heterogeneous catalysts have been developed to achieve the

selective cleavage of ether linkage in lignin. For example, some noble metal catalysts based on Pd [14–23], Ru [24,25], and Rh [26] have been proved efficient for the cleavage of C–O bond in various lignin model linkages. Whereas the scarcity and high cost of noble metals, non-noble metal based heterogeneous catalysts were perhaps more preferable for lignin conversion. A series of nickel-based catalysts such as heterogeneous Ni catalyst in-situ generated from Ni (CH₂TMS)₂(TMEDA) [27], Ni/SiO₂ [28–30], Ni/C [31–33], Ni/hydro-talcite (HTC) [34], raney Ni [35,36], titanium nitride-nickel nanocomposite (TiN–Ni) [37], NiMo (with or without sulfide) [38,39], Ni/niobic acid-activated carbon composites [40], NiAlOx [41], Ni/amorphous silica-alumina [42], Ni-based alloy catalysts [43–45], W₂C [46], and Mo-based catalyst [47,48] have been reported for reductive cleavage of ether linkage. However, the hydrogenation of the aromatic ring of the depolymerization products especially the phenolic fragments are usually inevitable to produce cyclohexanol or cycloalkanes, leading to unsatisfactory aromatic selectivity. Thus, more selective heterogeneous catalyst systems still need to be developed.

Iron has been featured as a very promising alternative to precious metals in catalysis because it is abundant, eco-friendly, relatively nontoxic, and inexpensive. Homogeneous iron catalysts such as ferric acetylacetonate [10] and fenton catalysts [49,50] have been used for

* Corresponding author.

E-mail addresses: lijiang@cup.edu.cn (J. Li), fuyao@ustc.edu.cn (Y. Fu).



Scheme 1. Selective hydrogenolysis of C–O bond of α -O-4 and β -O-4 lignin model linkages over heterogeneous iron catalysts. The oxidation of the α -carbon in the β -O-4 model compounds can generally lead to higher aromatics yields.

lignin depolymerization through reductive and oxidative cleavage, respectively. To date, the only heterogeneous iron catalyst used for lignin-derived C–O bond cleavage was bimetallic FeMoP catalyst, which was reported by Hicks et al. [51]. However, it suffered from very high reaction temperature (400 °C), and limited substrate scope was reported in their work.

Nitrogen-doped carbon material-supported iron catalysts have recently attracted much attention as ideal alternatives to noble metal catalysts in some important chemical reactions such as the oxygen reduction reaction (ORR) or nitroarene hydrogenation [52–54]. Notably, Beller et al. reported some pioneer work using heterogeneous iron catalysts for organic synthesis [54–60]. Inspired by their work, we recently successfully achieved some heterogeneous iron-catalyzed biomass conversions such as catalytic transfer hydrogenation of furfural to furfuryl alcohol [61] and selective hydrodeoxygenation of 5-hydroxymethylfurfural to 2,5-dimethylfuran [62]. In this work, selective cleavage of C–O bond of α -O-4 and β -O-4 lignin model linkages while preserving the aromatic nature was successfully achieved over heterogeneous iron catalysts (Scheme 1). The hydrogenolysis of α -O-4 model linkage showed that the catalyst prepared by the pyrolysis of iron(II) acetate and 1,10-phenanthroline on activated carbon at 800 °C was the most active heterogeneous iron catalyst, affording phenol and toluene with yields of 95% and 90%, respectively at 240 °C and 2 MPa H_2 . The aromatics selectivity is found to be much higher than that obtained over noble metal catalysts. For the β -O-4 linkage, we found that the vicinal –OH group was essential for the iron-catalyzed hydrogenolysis of C–O bond. In addition, the oxidation of the α -carbon in the β -O-4 model compounds could significantly decrease the bond dissociation energy

(BDE) of the ether linkage, giving hydrogenolysis products in moderate to excellent yields.

2. Experimental

2.1. List of chemicals

Benzyl phenyl ether (98%), guaiacol (98%), syringol (98%), ethylbenzene (99%), acetophenone (98.5%), 4'-methoxyacetophenone (99%), 1-ethyl-4-methoxybenzene (98%), 4-allylanisole (98%), 1-(4-methoxyphenyl)propan-1-one (97%), 1-phenylethane-1,2-diol (98%), 2-phenylethyl alcohol (98%), 1-phenylethanol (98%), styrene (99%), 2-hydroxy-1-phenylethanone (98%), iron(II) acetate anhydrous (90%), 1,10-phenanthroline (99%), 2,2'-bipyridine (99%), 2,2':6',2''-terpyridine (98%), hemin (95%), and activated carbon were purchased from TCI. Iron(III) acetylacetonate (98%) was purchased from J&K Chemical. 8-hydroxyquinoline (99.5%), phenylglycine (97%), cobalt(II) acetate tetrahydrate (99.5%), nickel(II) acetate tetrahydrate (98%), toluene (99.5%), phenol (99%), benzyl alcohol (98%) were purchased from Sinopharm Chemical Reagent Co. Ltd. Metal-oxide supports such as TiO_2 (99.99%), SiO_2 (99.8%), and Al_2O_3 (99.9%) were purchased from Aladdin Reagent Co. Ltd. Ru/C and Pd/C with 5% metal loading, and $H_2PtCl_6 \cdot 6H_2O$ (metal content > 38%) were purchased from Shanghai Jiuling Chemical Co. Ltd. The β -O-4 lignin model compounds were synthesized according to previous literature. The synthetic procedure and the 1H NMR spectra can be found in the Supporting Information.

2.2. Catalyst preparation

The catalyst was prepared by a simultaneous pyrolysis of metal precursors and nitrogen precursors on supports at a pyrolysis temperature ranged from 400 to 1000 °C as previous literature [61–63]. A typical procedure for catalyst preparation is described as follows: iron precursor (0.5 mmol) and corresponding ligands were added to ethanol (50 mL) under vigorously stirring at room temperature. Then activated carbon (1 g) was added into the solution, and the mixture was stirred at 60 °C for 15 h, followed by rotary evaporation at 30 °C. The obtained solid was ground into fine powder and then pyrolyzed under an Ar atmosphere with a gas flow rate of 100 mL min^{-1} in a tubular furnace. The as-prepared catalysts were denoted as Fe-Ln/S-T, in which Ln represents the type of nitrogen precursor, S represents the type of support, and T represents the pyrolysis temperature. The catalyst prepared from hemin was denoted as 6/C-800 (see Fig. S1 in the Supporting Information for more details).

Pt/C catalyst with 5% metal loading were prepared by an impregnation method using $H_2PtCl_6 \cdot 6H_2O$ as precursor. 133.5 mg $H_2PtCl_6 \cdot 6H_2O$ was first dissolved in 50 mL ethanol and then 1 g activated carbon was added. The mixture was stirred at 50 °C for 4 h followed by rotary evaporation at 30 °C. Obtained solid was ground into fine powder, and then pyrolyzed under a flowing gas mixture of 5 vol% H_2/Ar with a gas flow rate of 100 mL min^{-1} in a tubular furnace at 280 °C for 2 h.

2.3. Lignin extraction and oxidation

The procedure for the extraction of organosolv lignin from birch sawdust was described as follows: 50 g birch sawdust was mixed with 1:1 ethanol- H_2O (300 mL), and then the mixture was transferred to the autoclave. After purging the reactor with N_2 , the reactor was heated to 178 °C with a ramp rate of 1.5 °C min^{-1} , and then held for 3.3 h. The result mixture was filtered, and then the filtrate was transferred to rotary evaporation to give organosolv lignin.

The oxidation of organosolv lignin was performed as previous literature [64]. To a 50 mL autoclave, 35 mg of organosolv lignin and 1 mg of 4-acetamido-TEMPO were added. Subsequently, solutions of

1.5 μL of nitric acid (67%) in 1 mL acetonitrile, 1 μL of hydrochloric acid (37%) in 1 mL of acetonitrile, and 10 mL of acetonitrile and 100 μL of water were added. The autoclave was purged with oxygen gas. The oxygen pressure was adjusted to 1 MPa. The reaction mixture was stirred at 65 $^{\circ}\text{C}$ for 48 h, and then solvent was evaporated by rotary evaporation. The residue was washed by 1:1 water-THF solvent mixture, and then transferred to the autoclave for subsequent iron-catalyzed hydrogenolysis reaction.

2.4. Catalyst characterization

XPS was obtained with an X-ray photoelectron spectrometer (ESCALAB250, Thermo-VG Scientific, USA) using monochromatized AlK α radiation (1486.92 eV). For the fitting of the XPS results, Shirley type background subtraction is applied and charge correction is performed with reference to C 1s at 284.6 eV. $-(\text{N}\cdots\text{Fe})$ at 399.6 eV, pyrrolic N at 400.8 eV, and a combination of quaternary and graphitic N at 402 eV, N-Ti species at 396.8 eV. The FWHM is fixed as 1.5 eV except N-Ti species (about 2 eV). FT-IR spectra were recorded on a Nicolet 8700 FT-IR spectrometer, and the samples were prepared by the KBr pellet method. XRD analysis was conducted on an X-ray diffractometer (TTR-III, Rigaku Corp., Japan) using Cu K α radiation ($\lambda = 1.54056 \text{ \AA}$). The data were recorded over 2θ ranges of 10–70 $^{\circ}$. Nitrogen adsorption measurements were performed using an ASAP2020 M adsorption analyzer which reports adsorption isotherm, specific surface area and pore volume automatically. The Brunauer-Emmett-Teller (BET) equation was used to calculate the surface area in the range of relative pressures between 0.05 and 0.20. The pore size was calculated from the adsorption branch of the isotherms using the thermodynamic based Barrett-Joyner-Halenda (BJH) method. H $_2$ -TPR was conducted on a Quanta Chembet chemisorption instrument with a thermal conductivity detector (TCD). Approximately 100 mg sample was loaded in a quartz reactor and then heated to 800 $^{\circ}\text{C}$ with a heating ramp rate of 10 $^{\circ}\text{C min}^{-1}$ in a stream of 5% H $_2$ /Ar with a total flow rate of 50 mL min^{-1} . More details about catalyst characterization results can be found in Supporting Information.

2.5. Experimental procedure

The catalytic hydrogenolysis of lignin model compounds was performed using a 50 mL Zr-alloy autoclave provided by Anhui Kemi Machinery Technology Co., Ltd. For a typical procedure, lignin model compounds (0.5 mmol or 1 mmol) or organosolv lignin (35 mg), heterogeneous Fe catalyst (100 mg), and solvent (20 mL) were added into the autoclave with a quartz lining. After purging the reactor with H $_2$, the reaction was conducted with 1 MPa H $_2$ (at room temperature) at 240 $^{\circ}\text{C}$ for 12 h with a stirring speed of 800 rpm. After reaction, internal standards are added to the product solution, and then the liquid products were analyzed by using both GC and GC-MS. For the conversion of α -O-4 lignin model compound, 2-phenylethanol is used as internal standard to determine the yields of benzyl alcohol and phenol, and dodecane is used to determine the yield of toluene. For the conversion of β -O-4 lignin model compounds, benzyl alcohol and dodecane are used as internal standards to determine the yields of phenolic fragments and aromatic fragments, respectively. A representative GC spectrum can be seen in Fig. S11 in supporting information. GC-MS analyses were performed on an Agilent 7890 Gas Chromatograph equipped with a DB-WAXETR 30 m \times 0.25 mm \times 0.25 mm capillary column (Agilent) or a HP-5MS 30 m \times 0.25 mm \times 0.25 mm capillary column (Agilent). Although HP-5MS column is unsuitable for the determination of products yields due to the low polarity, it can be used to confirm whether some complex lignin model compounds were completely converted. The GC was directly interfaced to an Agilent 5977 mass selective detector (EI, 70 eV). The following GC oven temperature programs were used: 40 $^{\circ}\text{C}$ hold for 1 min, ramp 5 $^{\circ}\text{C min}^{-1}$ to a temperature of 120 $^{\circ}\text{C}$, and then ramp 10 $^{\circ}\text{C min}^{-1}$ to 300 $^{\circ}\text{C}$ and hold for 5 min. To get the

representative GC spectrum of gaseous products, the gaseous phase was collected and injected into a Fuli 9790II Gas Chromatograph equipped with a TDX-01 packed column and a thermal conductivity detector (TCD) through a six-way valve to analyze the composition.

The C–O cleavage of the lignin model compounds generally produce two fragments. One is aromatic fragment such as ethylbenzene or acetophenone. The other one is phenolic fragment. The carbon balance of phenolic fragment is always higher than aromatic fragment.

In the case of the conversion of α -O-4 lignin model compounds, the conversion and the yield were calculated as follows,

$$\text{Conversion} = (1 - (\text{moles of substrates after reaction}) / (\text{moles of substrates in the starting materials})) \times 100\%$$

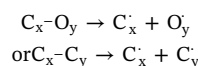
$$\text{Yield} = (\text{mole of each fragment product after reaction}) / (\text{moles of substrates in the starting materials}) \times 100\%$$

In the case of the conversion of β -O-4 lignin model compound, the boiling point of the substrates are too high to be detected in the GC-spectrum. Thus, the conversion of the substrates is not determined. The yield was calculated as follows,

$$\text{Yield} = (\text{mole of each fragment product after reaction}) / (\text{moles of substrates in the starting materials}) \times 100\%$$

2.6. DFT calculation method

Lignin model compounds and their corresponding radicals were fully optimized with the 6–311 + + G(d,p) basis set using Gaussian 03 software. Single-point energy calculations were performed at the same level of theory. The homolytic C–O or C–C bond-dissociation energies (BDEs) of the model compounds were estimated from the expression:



The C–O or C–C BDEs were calculated as follows:

$$\text{BDE} = \text{H}(\text{C}_y^{\cdot}) + \text{H}(\text{O}_y\text{orC}_y^{\cdot}) - \text{H}(\text{C}_x - \text{O}_y\text{orC}_x - \text{C}_y)$$

where H(i)s are the single-point energies of different species i at 298 K.

The BDEs represent the bond strength of the C–C or C–O linkages, so that they are compared to explain the different reactivities of the model compounds [28].

3. Results and discussion

3.1. Catalyst screening for reductive cleavage of C–O bond in α -O-4 lignin model compounds

The hydrogenolysis of α -O-4 lignin model compound, benzyl phenyl ether, in a water-tetrahydrofuran (THF) solvent mixture was selected as a model reaction to screen the best heterogeneous iron catalyst (Table 1). A glass vial was used to exclude the influence of the reactor body. In the blank test, phenol and benzyl alcohol were generated via hydrolysis pathway [29]. The protons existed in the hot water-THF system could be the acid catalyst for the hydrolysis reaction. Despite the reaction was performed under H $_2$, no toluene was detected, indicating that the hydrogenolysis reaction was unlikely to occur without any catalyst. To our delight, the iron catalyst prepared from Fe-phenanthroline (L1) complex exhibited excellent catalytic performance towards the hydrogenolysis reaction. The yields of phenol and toluene reached 95% and 90%, respectively, and the yield of hydrolysis product, benzyl alcohol, was only 5%. Only trace yield of CO $_2$ could be detected in the GC spectrum of gaseous phase (Fig. S12), indicating that very small amount of carbon is converted into gas phase. Under identical reaction condition, the hydrogenolysis of benzyl alcohol (11) afforded 25% yield of toluene and 10% yield of benzaldehyde at 40% conversion (see entry 1, Table 4), suggesting that toluene was more likely to be generated by direct hydrogenolysis of benzyl phenyl ether rather than the hydrolysis of benzyl phenyl ether to benzyl alcohol

Table 1
Catalyst screening for C–O bond cleavage of α -O-4 lignin model compound^a.

Entry	Catalysts	T °C	P MPa	Conversion [%]	Yield [%] ^b		
					a	b	c
1	–	240	2	70	61	0	53
2	Fe-L1/C-800	240	2	99	95	90	5
3	Fe-L1/C-800	220	2	84	65	68	3
4	Fe-L1/C-800	200	2	34	30	21	1
5	Fe-L1/C-800	240	1	98	90	57	23
6	Fe-L2/C-800	240	2	75	71	44	20
7	Fe-L3/C-800	240	2	96	93	73	14
8	Fe-L4/C-800	240	2	66	59	38	15
9	Fe-L5/C-800	240	2	69	58	28	19
10	6/C-800	240	2	99	94	89	5
11	Fe(III)-L1/C-800 ^c	240	2	95	88	84	5
12	Fe-L1/C-1000	240	2	86	72	64	6
13	Fe-L1/C-600	240	2	89	85	53	25
14	Fe-L1/C-400	240	2	42	28	12	9
15	Fe-L1/TiO ₂ -800	240	2	17	15	6	11
16	Fe-L1/SiO ₂ -800	240	2	68	55	40	9
17	Fe-L1/Al ₂ O ₃ -800	240	2	72	59	13	42
18	L1/C-800	240	2	90	80	9	68
19	Fe/C-800	240	2	71	67	19	31
20	Fe	240	2	83	73	3	65
21	L1	240	2	10	10	3	6
22	Fe-L1	240	2	9	8	3	4
23	C	240	2	100	84	5	74
24	Co-L1/C-800	240	2	92	87	60	18
25	Ni-L1/C-800	240	2	86	81	60	4
26 ^d	Ru/C ^g	240	2	97	n.d. ^h	n.d.	n.d.
27 ^e	Pd/C ^g	240	2	98	n.d.	n.d.	n.d.
28 ^f	Pt/C ^g	240	2	77	53	71	n.d.

^a Reaction conditions: 1 mmol benzyl phenyl ether, 1:1 water-THF (20 mL), 0.1 g iron catalyst, $t = 12$ h. The molar ratio of metal/benzyl phenyl ether was kept at 5.6 mol%.

^b GC yield.

^c Iron(III) acetylacetonate was used as iron precursor.

^d Ring-hydrogenation products are detected as major by-products: cyclohexanol (13%), cyclohexanone (20%), cyclohexane (12%), methylcyclohexane (34%), cyclohexylmethanol (31%).

^e Major by-products: cyclohexanol (82%), cyclohexanone (7%), cyclohexane (3%), methylcyclohexane (63%).

^f 2% yield of cyclohexanol, 4% yield of methylcyclohexane, and 8% yield of cyclohexane are obtained as major-products.

^g The metal loading was 5 wt%.

^h n.d. = not detected.

followed by deoxygenation. Moreover, we did not observe any ring-hydrogenated products such as cyclohexanol or methyl cyclohexane, suggesting that the aromatic rings were well reserved during the iron-catalyzed C–O bond cleavage. This chemoselectivity was highly advantageous for the concept of catalytic valorization of lignin to aromatic chemicals.

Significant decreases in ether conversion and hydrogenolysis products yields were observed when experiments were performed at lower reaction temperatures and hydrogen pressures (entries 2–5). The iron catalyst prepared from the native iron complex (6/C-800) afforded similar yields of hydrogenolysis products, but catalysts prepared from other nitrogen precursors exhibited much more inferior hydrogenolysis activities (entries 6–10).

To explore the reason for the outstanding catalytic performance of Fe-L1/C-800 catalyst, the iron catalysts have been characterized by various technologies such as XPS, XRD, BET, and H₂-TPR. As this kind of iron catalysts has represented excellent activity for various chemical conversions, the presence of an Fe-N_x type structure as the active center is generally accepted [65,66], which can be realized by the XPS analysis. The N 1s XPS spectra of Fe-L1/C-800 catalyst, and some other inferior iron catalysts such as Fe-L2/C-800, Fe-L5/C-800, and Fe-L1/TiO₂-800 catalysts are shown in Fig. 1. In general, the peaks in the N1s

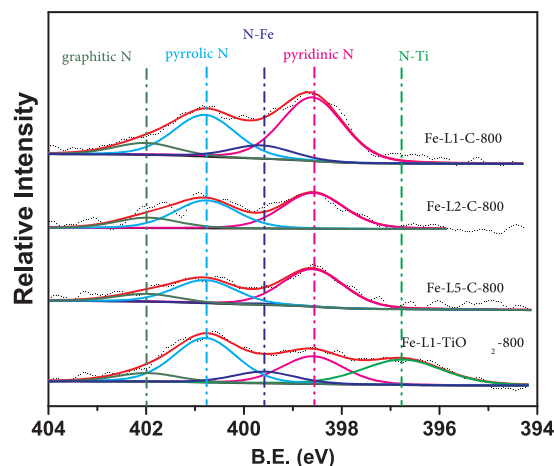


Fig. 1. N 1s XPS spectra of Fe-L1/C-800, Fe-L2/C-800, Fe-L5/C-800, and Fe-L1/TiO₂-800 catalysts.

XPS spectra can be divided into four species: pyridinic N at 398.6 eV, N coordinated to Fe (N...Fe) at 399.6 eV, pyrrolic N at 400.8 eV, and a combination of quaternary and graphitic N at 402 eV [67,68]. For the Fe-L1/TiO₂-800 catalyst, N-Ti species can be detected at 396.8 eV [69]. The results for N speciation of various iron catalysts are listed in table S1 (see supporting information). For iron catalysts prepared from different ligands, it can be clearly seen that a certain amount of N...Fe species can be found in relatively more active iron catalysts such as Fe-L1/C-800, Fe-L3/C-800, and 6/C-800 catalysts, and it reached the highest value for Fe-L1/C-800 catalyst. By contrast, extremely low percentage content (2.6% of total N contents) of N...Fe species were found in Fe-L5/C-800 catalyst, and no N...Fe species were found in the XPS spectra of Fe-L2/C-800 and Fe-L4/C-800 catalysts. These results confirm that the presence of N...Fe species is important for the HDO activities of iron catalysts. In addition, for the Fe-L5/C-800 catalyst, FeO_x species, which are adverse for the catalytic performance of iron catalysts [61], can be detected as shown in its XRD pattern (Fig. 2). Extremely weak peaks of FeN_x, Fe₃C, and metallic Fe can be found in the XRD pattern of Fe-L1/C-800 catalyst, indicating that all the iron species are homogeneously dispersed on the support. The excellent catalytic performance of Fe-L1/C-800 catalyst suggested that this well-dispersion of iron species onto carbon support is favorable for the HDO reaction.

The iron precursor iron(II) acetate could be replaced by iron(III) acetylacetonate without significant loss of catalytic activity (entry 11). 0.88 at% of N...Fe species can be observed in its XPS spectrum. The effect of pyrolysis temperature indicated that the optimal pyrolysis temperature was 800 °C (entries 12–14). At pyrolysis temperature lower than 800 °C, the iron precursors are not incorporated into carbon support to form active sites [54]. However, when the pyrolysis temperature was raised to 1000 °C, the total N content decreased sharply to 0.34 at% (2.65 at% at 800 °C), suggesting that the N...Fe species were collapsed to release nitrogen. In addition, inactive Fe₂O₃ phase is found in its XRD pattern (see Fig. S5 in the supporting information).

Iron catalysts prepared on metal oxides exhibited inferior catalytic performance than that on activated carbon (entries 15–17). Carbon is usually the best support to prepare highly active Fe-N catalysts. The reasons include: 1) catalysts prepared from carbon usually have the highest BET surface area (Table 2), thus leading to the exposure of more active sites on the catalyst surface to catalyze reactions; 2) the doping nitrogen donates more electrons to the carbon support to facilitate redox reactions [70]; 3) N-doped carbon materials are recommended as “solid ligands” to bind metal nanoparticles to form structures mimicked homogeneous metal complexes with N ligands [71].

The poor catalytic performances of L1/C-800, Fe/C-800, iron(II)

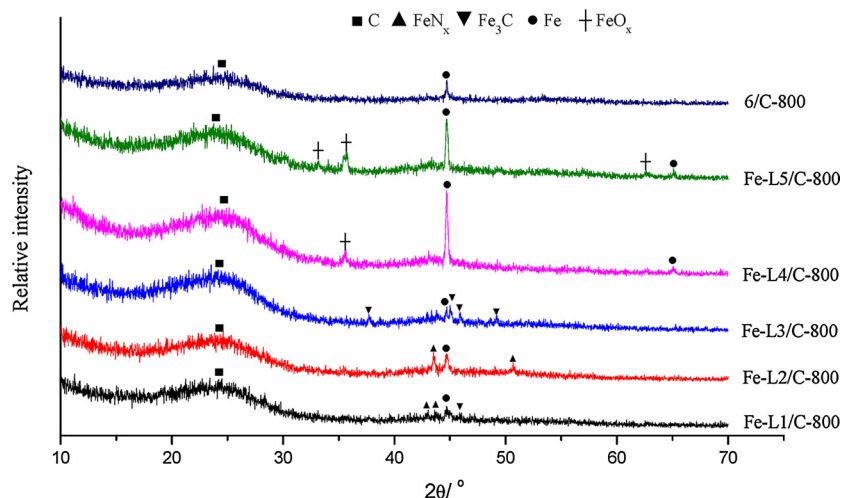


Fig. 2. The XRD patterns of various iron catalysts prepared from different nitrogen precursors.

Table 2

Textural properties of iron catalysts prepared from different supports.

Entry	Catalysts	S_{BET} [m ² /g]	V_p [cm ³ /g]	Pore Size [nm]
1	Fe-L1/C-800	830	0.89	4.27
2	Fe-L1/TiO ₂ -800	52	0.05	3.62
3	Fe-L1/SiO ₂ -800	245	0.70	11.40
4	Fe-L1/Al ₂ O ₃ -800	43	0.08	6.97

acetate (Fe), 1,10-phenanthroline (L1), iron complex (Fe-L1), and carbon support confirmed that the simultaneous pyrolysis of iron precursor and nitrogen precursor on a carbon support was critical to the hydrogenolysis activity of the iron catalysts. The replacement of the metal center Fe with Co or Ni would lead to inferior catalytic activity.

The catalytic performance of iron catalysts are also compared with noble metal catalysts (entries 26–28). Ring-hydrogenation products are detected as major by-products when Ru/C and Pd/C catalysts are used. Pt/C catalyst afforded 53% yield of phenol and 71% yield of toluene, which is lower than that of Fe-L1/C-800 catalyst. In addition, the solvent THF will be converted to ring-opening products such as butanol or butanediol over noble metal catalysts. By contrast, the cyclic ether solvent THF remained stable over iron catalysts. Thus, the iron catalyst represented better catalytic performance towards the hydrogenolysis of α -O-4 lignin model compound than noble metal catalysts.

To explore the reaction pathway for the conversion of α -O-4 lignin model compound, the time course for the hydrogenolysis of benzyl phenyl ether over Fe-L1/C-800 catalyst was investigated (Fig. 3). It was shown that the substrate benzyl phenyl ether was completely consumed after 12 h, and highly selective hydrogenolysis of the α -O-4 linkage was achieved to afford phenol and toluene as main products. The yield of benzyl alcohol was below 5% during the reaction. Owing to the large excess of hydrogen, the hydrogenolysis of benzyl phenyl ether was a pseudo-first order reaction with a reaction rate constant of 0.30825 at 513 K (Fig. S13).

To sum up, the reaction pathway for the conversion of α -O-4 lignin model compound is shown in Scheme 2. When the reaction is performed without iron catalysts, the α -O-4 lignin model compound will be hydrolyzed to phenol and benzyl alcohol catalyzed by the protons existed in the hot water-THF system. In contrast, the use of Fe-L1/C-800 catalyst led to the generation of phenol and toluene by direct hydrogenolysis of ether linkage. Toluene is unlikely to be generated by the hydrolysis of α -O-4 lignin model compound followed by hydrogenolysis because Fe-L1/C-800 catalyst is ineffective at catalyzing the conversion of benzyl alcohol to toluene.

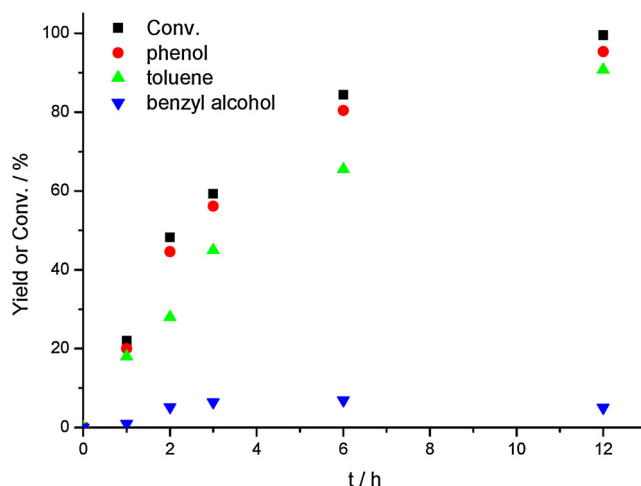
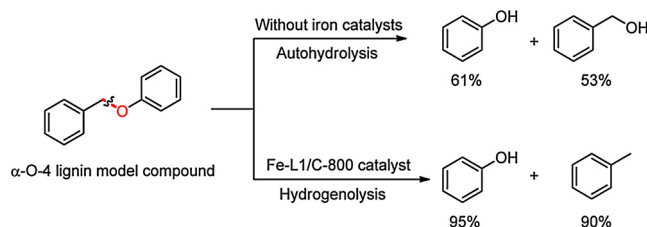


Fig. 3. The time course for the hydrogenolysis of benzyl phenyl ether over Fe-L1/C-800 catalyst. Reaction condition: 1 mmol benzyl phenyl ether, 1:1 water-THF (20 mL), 0.1 g Fe-L1/C-800 catalyst, 2 MPa H₂, T = 240 °C.

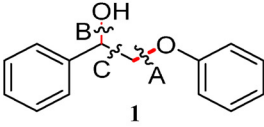
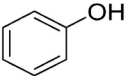
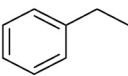
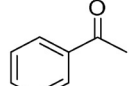
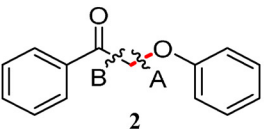
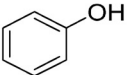
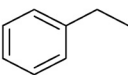
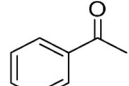
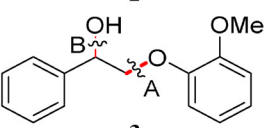
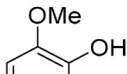
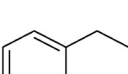
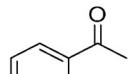
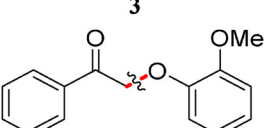
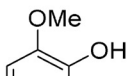
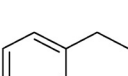
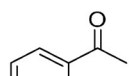
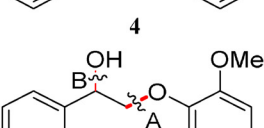
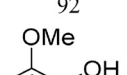
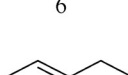
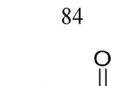
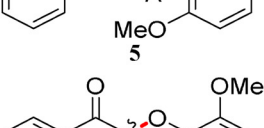
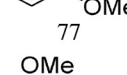
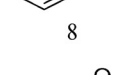
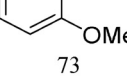
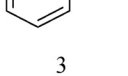
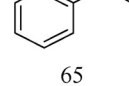
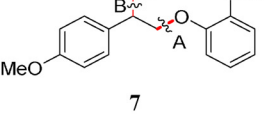
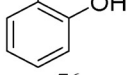
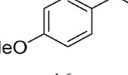
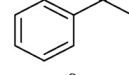
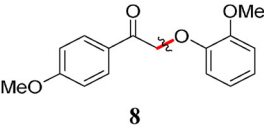
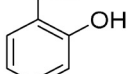
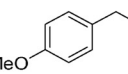
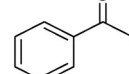
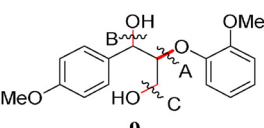
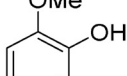
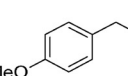
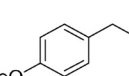


Scheme 2. Different reaction pathways for the conversion of α -O-4 lignin model compound with or without iron catalysts in a H₂O-THF solvent mixture.

3.2. Reductive cleavage of C–O bond in β -O-4 lignin model compounds

The excellent catalytic performance of Fe-L1/C-800 catalyst in the hydrogenolysis of α -O-4 model linkage inspired us to further explore the heterogeneous iron-catalyzed hydrogenolysis of β -O-4 linkage (Table 3), which is the most predominant type of ether linkages in native lignin. The simplest model compound of β -O-4 linkage, 2-phenoxy-1-phenylethanol (compound 1), could be cleaved to phenol, ethylbenzene, and acetophenone with yields of 43%, 40%, and 3%, respectively. The unsatisfactory yields of hydrogenolysis products could be partially attributed to the generation of phenethoxybenzene (compound 12, see Table 4) as the by-product with 20% yield, for which the

Table 3
The hydrogenolysis of β -O-4 lignin model compounds over Fe-L1/C-800 catalyst^a.

Substrate	BDE KJ/mol	Conv. [%] ^b	Yield [%] ^b		
	A: 266 B: 344 C: 302	N.D.	 43	 40	 3 ^c
	A: 208 B: 317	>99	 >99	 5	 90
	A: 236 B: 338	N.D.	 84	 65	 7
	186	N.D.	 92	 6	 84
	A: 237 B: 353	N.D.	 77	 68	 8
	171	N.D.	 73	 3	 65
	A: 242 B: 344	N.D.	 76	 46	 8
	186	N.D.	 93	 5	 85
	A: 228 B: 336 C: 388	N.D.	 84	 5	 59
	A: 162 B: 382	N.D.	 82	 40	 13

^aReaction conditions: 0.5 mmol β -O-4 lignin model compounds, 1:1 water-THF (20 mL), 0.1 g Fe-L1/C-800 catalyst, 1 MPa H₂, T = 240 °C, t = 12 h. N. D. = not determined.

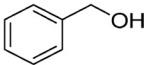
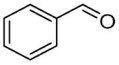
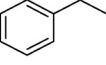
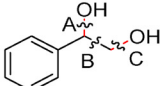
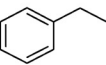
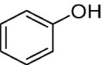
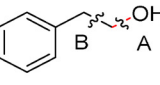
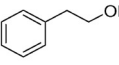
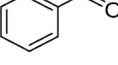
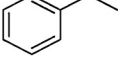
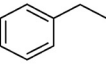
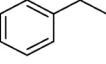
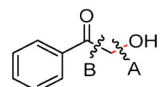
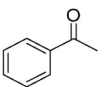
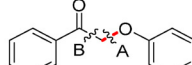
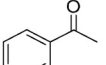
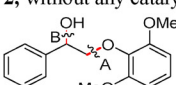
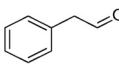
^bDetermined by GC.

^cPhenethoxybenzene could be observed as the by-product with 20% yield.

cleavage of ether linkage was unlikely to occur even at a reaction temperature of 290 °C (Table 4). However, the BDE of ether linkage in **12** (261 kJ/mol) was slightly lower than that in **1** (266 kJ/mol), suggesting that the cleavage of ether linkage in **12** should be theoretically easier to occur. This contradiction indicated that the vicinal -OH

group was essential for the iron-catalyzed cleavage of C–O bond, which can be further confirmed by the different reactivity of 1-phenylethane-1,2-diol (compound **13**, see Table 4) and 2-phenylethanol (compound **14**, see Table 4). Total conversion of **13** could be achieved over Fe-L1/C-800 catalyst, giving 29% yield of **14**, 13% yield of benzaldehyde, and

Table 4
Heterogeneous iron-catalyzed cleavage of various molecules to confirm the reaction pathway^a.

Entry	Substrate	BDE KJ/mol	T [°C]	T [h]	Conv. [%] ^b	Yield [%] ^b
1	 11	-	240	12	40	 10  25
2		261	240	12	N.D.	 0.4
3	 13	A: 346 B: 281 C: 398	240	12	>99	 3  3
4	 14	A: 390 B: 293	240	12	3	 29  13  50
5	 15	335	240	12	>99	 90  4
6	 16	-	240	12	>99	 >99
7	 17	A: 338 B: 294	240	12	22	 17
8	 2, without any catalyst	A: 208 B: 317	240	12	N.D.	 15  17
9	 5, without any catalyst	A: 237 B: 353	240	12	N.D.	 5  12

^aReaction conditions: 0.5 mmol substrate, 1:1 water-THF (20 mL), 0.1 g Fe-L1/C-800 catalyst, 1 MPa H₂, T = 240 °C, t = 12 h. N.D. = Not determined.

^bDetermined by GC.

50% yield of ethylbenzene. In contrast, only 2% yield of ethylbenzene was obtained from **14** with only 3% conversion. In addition, the C–C bond became weaker in the pinacol structure, so that the cleavage of C–C bond could be observed during the hydrogenolysis of **13**.

The cleavage of ether linkage in **1** was more favorable at a higher reaction temperature of 290 °C, giving 88% yield of phenol, 59% yield of ethylbenzene, and 25% yield of acetophenone. Acetophenone was probably formed by the hydrogenation of **1** to compound **2** followed by C–O bond cleavage rather than C–O bond cleavage followed by dehydrogenation of 1-phenylethanol (compound **15**, see Table 4) because **15** would be converted to ethylbenzene with 90% selectivity under identical reaction condition. Although it is hard to imagine that the dehydrogenation reaction can happen in a hydrogen atmosphere, the iron-catalyzed dehydrogenation reaction under H₂ has been proven in our latest work, where considerable yield of 2,5-diformylfuran was obtained from 5-hydroxymethylfurfural over Fe-L1/C-800 catalyst in THF [62]. In addition, 10% yield of benzaldehyde can be obtained from benzyl alcohol under identical reaction condition (entry 1, Table 4),

further confirming that the dehydrogenation reaction definitely occurred over heterogeneous iron catalysts under H₂. The high selectivity of ethylbenzene from **15** also explained why the major product from the hydrogenolysis of **1** is ethylbenzene. Owing to the high BDE for C–O bond in **15** (335 kJ/mol), we proposed that the reaction pathway for the conversion of **15** to ethylbenzene was the dehydration of **15** to styrene (compound **16**, see Table 4) followed by hydrogenation. This hypothesis is confirmed by the time course for the hydrogenolysis of **15** (Fig. S14), where 19.4% yield of styrene can be detected at 2 h and then be completely converted after 12 h.

The oxidation of the α -carbon in β -O-4 linkage has been previously proved to significantly weaken the ether bond, thus leading to more effective lignin degradation [12,64,72,73]. Hence, we further explored the iron-catalyzed hydrogenolysis of oxidative β -O-4 model compounds. The BDE of ether linkage decreased from 266 to 208 kJ/mol after the oxidation of the α -carbon in **1**, and the oxidative product (compound **2**) could be nearly quantitatively cleaved to yield aromatic products. The yield of ethylbenzene was only 5%, suggesting that

acetophenone was more stable than **15** under identical reaction condition. In addition, the calculation of BDE of C–C and C–O linkages in **1**, **2**, **13** and 2-hydroxy-1-phenylethanone (compound **17**, see Table 4) suggested that the oxidation of the α -carbon led to weaker C–O linkage and stronger C–C bond. Thus, the cleavage of C–O bond was more preferable than the cleavage of C–C bond in the oxidative β -O-4 model compounds, leading to higher carbon balance.

The iron-catalyzed C–O bond cleavage of some more complex β -O-4 model compounds was also explored. It was shown that the BDE of ether linkage in guaiacol-based β -O-4 model compound (compound **3**) was 30 kJ/mol lower than that in phenol-based β -O-4 model compound (compound **1**), so that **3** could be cleaved to aromatic compounds with higher yields. In addition, for these more complex β -O-4 model compounds, higher reaction temperature will lead to lower carbon balance. The oxidative product of **3** (compound **4**) can be cleaved to aromatic compounds with excellent yields.

The iron-catalyzed C–O bond cleavage in the syringol-based β -O-4 model compounds (**5**) was less effective than **3**, despite that the BDE of the ether linkage was similar. In addition, unexpected low yields of hydrogenolysis products were obtained for the conversion of the oxidative product of **5** (compound **6**), despite the BDE of the ether linkage was only 171 kJ/mol. The steric hinderance caused by two *o*-methoxy groups was probably the main reason for the ineffective hydrogenolysis of the ether linkage. The presence of *p*-methoxy group in guaiacol-based β -O-4 model compound (**7**) led to slightly higher BDE of C–O bond (as compared to **3**), thus affording lower hydrogenolysis products. In comparison, the oxidative product of **7** (compound **8**) could be cleaved to aromatic compounds with excellent yields.

The C–O bond cleavage of the β -O-4 lignin linkage of 1,3-dilignol model compounds was also examined. At a reaction temperature of 240 °C, **9** was cleaved to guaiacol, 1-ethyl-4-methoxybenzene, and 1-methoxy-4-propylbenzene with yields of 84%, 5%, and 59%, respectively. When the reaction temperature was raised to 290 °C, the yields of aromatic fragments decreased significantly while the yields of phenolic fragments remained nearly unchanged. The yields of aromatic fragments were always lower than those of phenolic fragments during the depolymerization of lignin-derived compounds, which was likely due to condensation reactions [74]. The cleavage of C–C bond in the pinacol structure could be observed in the hydrogenolysis of the oxidative product of **9** (compound **10**), giving 40% yield of 1-(4-methoxyphenyl)ethanone and 13% yield of 1-(4-methoxyphenyl)propan-1-one.

The reaction pathways for the conversion of native and oxidative β -O-4 lignin dimers **1** and **2** over Fe-L1/C-800 catalyst were further explored. The blank tests demonstrated that the iron catalyst played an important role during the hydrogenolysis of β -O-4 lignin dimers (entries 9 and 10, Table 4). In addition, the time course for the hydrogenolysis of **1** and **2** over Fe-L1/C-800 catalyst was shown in Fig. 4. For the conversion of native lignin dimer **1**, the main pathway is the hydrogenolysis of **1** to form phenol and 1-phenylethanol, which was further converted to ethylbenzene through deoxygenation. 1-phenylethanol was not observed during the reaction, which was probably due to the rapid hydrogenolysis of 1-phenylethanol to ethylbenzene (Fig. S14). Two other pathways can also be observed: (a) the deoxygenation of **1** to phenethoxybenzene with yield of ca. 20%, which was unlikely to be further depolymerized to monomers over iron catalysts; (b) the dehydrogenation of **1** to **2** followed by hydrogenolysis to form phenol and acetophenone with yield of < 10%. The direct hydrogenolysis of ether linkage is more preferable in the depolymerization of more complex native lignin dimers such as **3**, **5**, **7** and **9** due to the lower BDE of ether linkages, and thus led to higher yields of monomers. The reaction pathway for the conversion of oxidative lignin dimer such as **2** is much simpler. The dimers can be depolymerized to monomers with excellent yields through direct hydrogenolysis. The as-mentioned reaction pathways are shown in Scheme 3.

Finally, we also initiated some preliminary studies about iron-catalyzed conversion of lignin. Organsolv lignin was first used in this

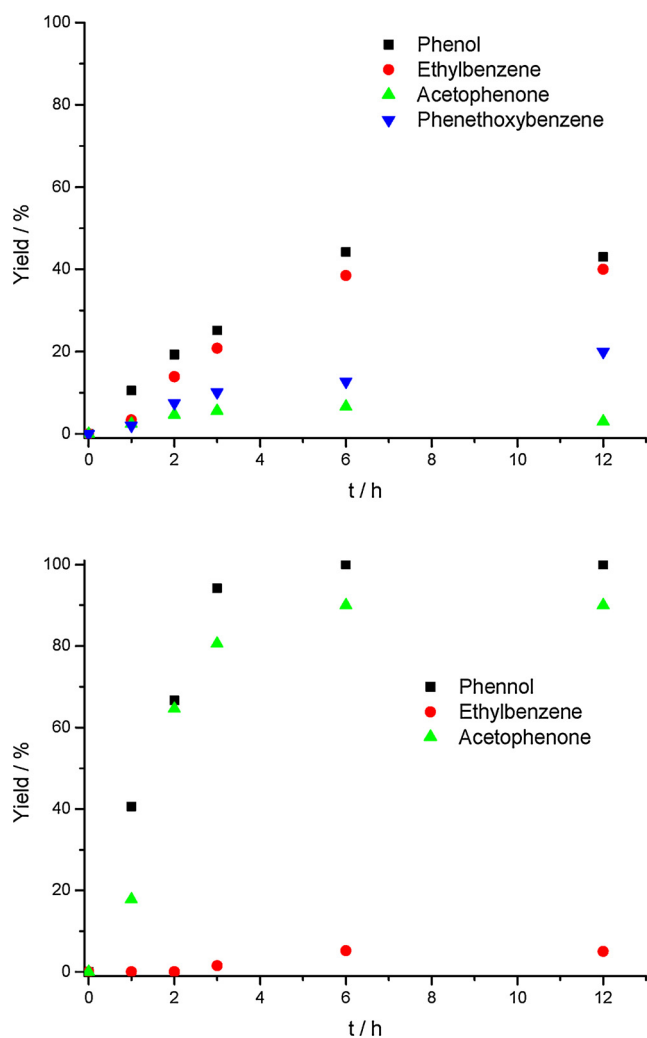
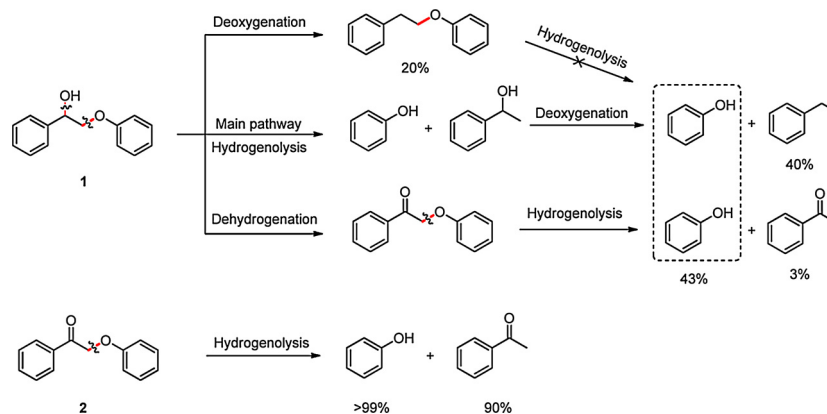


Fig. 4. The time course for the hydrogenolysis of **1** and **2** over Fe-L1/C-800 catalyst. Reaction condition: 0.5 mmol substrate, 1:1 water-THF (20 mL), 0.1 g Fe-L1/C-800 catalyst, 1 MPa H₂, T = 240 °C. **2** was completely consumed after 6 h, but incomplete conversion of **1** was observed even after 12 h.

section, and the details for its extraction can be found in experimental section. In addition, the oxidation of as-prepared lignin was also carried out according to previous literature [64]. To our disappointment, no monomers were detected after the reaction of two types of lignin with Fe-L1/C-800 catalyst. The GPC analysis (Fig. S15) showed that the native lignin treated by Fe-L1/C-800 catalyst tends to high molecular scope, which probably due to the polymerization of native lignin [73,74]. We proposed that the relatively low catalytic activity of Fe and the steric effect observed in the iron-catalyzed hydrogenolysis of β -O-4 model linkage was the main reason for the poor reactivity during lignin conversion, which led to difficult contact of the heterogeneous iron catalyst with the ether linkage in the lignin. Nonetheless, we believe that the unique chemoselectivity of the iron catalyst will hold great potential for the conversion of lignin to aromatics. The preparation of some iron-based alloy catalysts such as PtFe or PdFe catalysts maybe could improve the catalytic performance towards the conversion of native lignin while preserving the chemoselectivity of iron. The relevant investigations are currently ongoing in our laboratory.

4. Conclusion

In summary, we report that the selective cleavage of C–O bond in lignin model compounds without hydrogenation of aromatic ring can



Scheme 3. Reaction pathways for the conversion of native and oxidative β -O-4 lignin dimers **1** and **2** over Fe-L1/C-800 catalyst.

be successfully achieved through heterogeneous iron catalysis. The hydrogenolysis of α -O-4 model linkage shows that the iron catalyst prepared by the simultaneous pyrolysis of iron acetate and 1,10-phenanthroline on activated carbon at 800 °C is the most active iron catalyst, affording phenol and toluene with yields of 95% and 90%, respectively. For the β -O-4 linkage, the vicinal –OH group was essential for the iron-catalyzed hydrogenolysis of ether linkage. Moreover, the oxidation of the α -carbon in the β -O-4 model compounds can significantly decrease the bond dissociation energy (BDE) of ether linkage, leading to improved hydrogenolysis reactivity, thus giving depolymerization products in moderate to excellent yields.

Acknowledgements

This work was supported by Science Foundation of China University of Petroleum, Beijing (No. 2462014YJRC037, C201604), the National Natural Science Foundation of China (21702227) and the National Key Research and Development Program of China (No. 2016YFB0100201). We thank supercomputer center of USTC for computational support.

Appendix A. Supplementary data

Supplementary data associated with this article can be found, in the online version, at <http://dx.doi.org/10.1016/j.mcat.2018.03.014>.

References

- [1] G.W. Huber, S. Iborra, A. Corma, *Chem. Rev.* 106 (2006) 4044.
- [2] A. Corma, S. Iborra, A. Velty, *Chem. Rev.* 107 (2007) 2411.
- [3] J. Zakzeski, P.C.A. Bruijninx, A.L. Jongerius, B.M. Weckhuysen, *Chem. Rev.* 110 (2010) 3552.
- [4] A.G. Sergeev, J.F. Hartwig, *Science* 332 (2011) 439.
- [5] J.M. Nichols, L.M. Bishop, R.G. Bergman, J.A. Ellman, *J. Am. Chem. Soc.* 132 (2010) 12554.
- [6] A. Wu, B.O. Patrick, E. Chung, B.R. James, *Dalton Trans.* 41 (2012) 11093.
- [7] W. Huo, W. Li, M. Zhang, W. Fan, H. Chang, H. Jameel, *Catal. Lett.* 144 (2014) 1159.
- [8] S. Son, F.D. Toste, *Angew. Chem. Int. Ed.* 49 (2010) 3791.
- [9] S.K. Hanson, R. Wu, L.A. Silks, *Angew. Chem. Int. Ed.* 51 (2012) 3410.
- [10] Y. Ren, M. Yan, J. Wang, Z.C. Zhang, K. Yao, *Angew. Chem. Int. Ed.* 52 (2013) 12674.
- [11] M.C. Haibach, N. Lease, A.S. Goldman, *Angew. Chem. Int. Ed.* 53 (2014) 10160.
- [12] J.D. Nguyen, B.S. Matsuura, C.R.J. Stephenson, *J. Am. Chem. Soc.* 136 (2014) 1218.
- [13] R.G. Harms, I.L.E. Markovits, M. Drees, W.A. Herrmann, M. Cokoja, F.E. Kühn, *ChemSusChem* 7 (2014) 429.
- [14] X. Zhou, J. Mitra, T.B. Rauchfuss, *ChemSusChem* 7 (2014) 1623.
- [15] T.H. Parsell, B.C. Owen, I. Klein, T.M. Jarrell, C.L. Marcum, L.J. Hauptert, L.M. Amundson, H.I. Kenttämä, F. Ribeiro, J.T. Miller, M.M. Abu-Omar, *Chem. Sci.* 4 (2013) 806.
- [16] T.L. Lohr, Z. Li, T.J. Marks, *ACS Catal.* 5 (2015) 7004.
- [17] J.K. Kim, J.K. Lee, K.H. Kang, J.C. Song, I.K. Song, *Appl. Catal. A* 498 (2015) 142.
- [18] H.L. Fan, Y.Y. Yang, J.L. Song, Q.L. Meng, T. Jiang, G.Y. Yang, B.X. Han, *Green Chem.* 17 (2015) 4452.
- [19] G. Zhu, X. Ouyang, Y. Yang, T. Ruan, X. Qiu, *RSC Adv.* 6 (2016) 17880.
- [20] F. Gao, J.D. Webb, H. Sorek, D.E. Wemmer, J.F. Hartwig, *ACS Catal.* 6 (2016) 7385.
- [21] E. Paone, C. Espro, R. Pietropaolo, F. Mauriello, *Catal. Sci. Technol.* 6 (2016) 7937.
- [22] I. Klein, C. Marcum, H. Kenttämä, M.M. Abu-Omar, *Green Chem.* 18 (2016) 2399.
- [23] M. Wang, H. Shi, D.M. Camaioni, J.A. Lercher, *Angew. Chem. Int. Ed.* 56 (2017) 2110.
- [24] Y.B. Huang, L. Yan, M.Y. Chen, Q.X. Guo, Y. Fu, *Green Chem.* 17 (2015) 3010.
- [25] Z. Luo, Y. Wang, M. He, C. Zhao, *Green Chem.* 18 (2016) 433.
- [26] M. Chatterjee, T. Ishizaka, A. Suzuki, H. Kawanami, *Chem. Commun.* 49 (2013) 4567.
- [27] A.G. Sergeev, J.D. Webb, J.F. Hartwig, *J. Am. Chem. Soc.* 134 (2012) 20226.
- [28] J. He, C. Zhao, J.A. Lercher, *J. Am. Chem. Soc.* 134 (2012) 20768.
- [29] J. He, C. Zhao, D. Mei, J.A. Lercher, *J. Catal.* 309 (2014) 280.
- [30] J. He, L. Lu, C. Zhao, D. Mei, J.A. Lercher, *J. Catal.* 311 (2014) 41.
- [31] Q. Song, F. Wang, J. Cai, Y. Wang, J. Zhang, W. Yu, J. Xu, *Energy Environ. Sci.* 6 (2013) 994.
- [32] F. Gao, J.D. Webb, J.F. Hartwig, *Angew. Chem. Int. Ed.* 55 (2016) 1474.
- [33] J. Chen, F. Lu, X. Si, X. Nie, J. Chen, R. Lu, J. Xu, *ChemSusChem* 9 (2016) 3353.
- [34] M.R. Sturgeon, M.H. O'Brien, P.N. Ciesielski, R. Katahira, J.S. Kruger, S.C. Chmely, J. Hamlin, K. Lawrence, G.B. Hunsinger, T.D. Foust, R.M. Baldwin, M.J. Biddy, G.T. Beckham, *Green Chem.* 16 (2014) 824.
- [35] X. Wang, R. Rinaldi, *ChemSusChem* 5 (2012) 1455.
- [36] P. Ferrini, R. Rinaldi, *Angew. Chem. Int. Ed.* 53 (2014) 8634.
- [37] V. Molinari, C. Giordano, M. Antonietti, D. Esposito, *J. Am. Chem. Soc.* 136 (2014) 1758.
- [38] C. Zhang, J. Lu, X. Zhang, K. Macarthur, M. Heggen, H. Li, F. Wang, *Green Chem.* 18 (2016) 6545.
- [39] C.R. Kumar, N. Anand, A. Kloekhorst, C. Cannilla, G. Bonura, F. Frusteri, K. Barta, H.J. Heeres, *Green Chem.* 17 (2015) 4921.
- [40] S. Jin, Z. Xiao, X. Chen, L. Wang, J. Guo, M. Zhang, C. Liang, *Ind. Eng. Chem. Res.* 54 (2015) 2302.
- [41] X. Cui, H. Yuan, K. Junge, C. Topf, M. Beller, F. Shi, *Green Chem.* 19 (2017) 305.
- [42] J. Kong, B. Li, C. Zhao, *RSC Adv.* 6 (2016) 71940.
- [43] J. Zhang, H. Asakura, J. Rijn, J. Yang, P. Duchesne, B. Zhang, X. Chen, P. Zhang, M. Saeys, N. Yan, *Green Chem.* 16 (2014) 2432.
- [44] J. Zhang, J. Teo, X. Chen, H. Asakura, T. Tanaka, K. Teramura, N. Yan, *ACS Catal.* 4 (2014) 1574.
- [45] J. Zhang, Y. Cai, G. Lu, C. Cai, *Green Chem.* 18 (2016) 6229.
- [46] H.W. Guo, B. Zhang, Z.J. Qi, C.Z. Li, J.W. Ji, T. Dai, A.Q. Wang, T. Zhang, *ChemSusChem* 10 (2017) 523.
- [47] R. Ma, W.Y. Hao, X.L. Ma, Y. Tian, Y.D. Li, *Angew. Chem. Int. Ed.* 53 (2014) 7310.
- [48] T. Prasomsri, M. Shetty, K. Murugappan, Y. Román-Leshkov, *Energy Environ. Sci.* 7 (2014) 2660.
- [49] J. Zeng, C.G. Yoo, F. Wang, X. Pan, W. Vermerris, Z. Tong, *ChemSusChem* 8 (2015) 861.
- [50] J. Mottweiler, T. Rinesch, C. Besson, J. Buendia, C. Bolm, *Green Chem.* 17 (2015) 5001.
- [51] D.J. Rensel, S. Rouvimov, M.E. Gin, J.C. Hicks, *J. Catal.* 305 (2013) 256.
- [52] M. Lefèvre, E. Proietti, F. Jaouen, J.P. Dodelet, *Science* 324 (2009) 71.
- [53] G. Wu, K.L. More, C.M. Johnston, P. Zelenay, *Science* 332 (2011) 443.
- [54] R.V. Jagadeesh, A.E. Surkus, H. Junge, M.M. Pohl, J. Radnik, J. Rabeah, M. Beller, *Science* 342 (2013) 1073.
- [55] R.V. Jagadeesh, H. Junge, M. Beller, *ChemSusChem* 8 (2015) 92.
- [56] T. Stemmler, A. Surkus, M. Pohl, K. Junge, M. Beller, *ChemSusChem* 7 (2014) 3012.
- [57] R.V. Jagadeesh, G. Wienhöfer, F.A. Westerhaus, A.E. Surkus, M.M. Pohl, H. Junge, K. Junge, M. Beller, *Chem. Commun.* 47 (2011) 10972.
- [58] R.V. Jagadeesh, K. Natte, H. Junge, M. Beller, *ACS Catal.* 5 (2015) 1526.
- [59] R.V. Jagadeesh, H. Junge, M. Beller, *Nat. Commun.* 5 (2014) 4123.
- [60] X.J. Cui, Y.H. Li, S. Bachmann, M. Scalone, A. Surkus, K. Junge, C. Topf, M. Beller, *J. Am. Chem. Soc.* 137 (2015) 10652.
- [61] J. Li, J.L. Liu, H.J. Zhou, Y. Fu, *ChemSusChem* 9 (2016) 1339.
- [62] J. Li, J.L. Liu, H.Y. Liu, G.Y. Xu, J.J. Zhang, J.X. Liu, G.L. Zhou, Q. Li, Z.H. Xu, Y. Fu, *ChemSusChem* 10 (2017) 1436.
- [63] R.V. Jagadeesh, T. Stemmler, A.E. Surkus, H. Junge, K. Junge, M. Beller, *Nat. Protoc.* 10 (2015) 548.

- [64] A. Rahimi, A. Ulbrich, J.J. Coon, S.S. Stahl, *Nature* 515 (2014) 249.
- [65] M. Lefèvre, E. Proietti, F. Jaouen, J.P. Dodelet, *Science* 324 (2009) 71.
- [66] C.H. Choi, W.S. Choi, O. Kasian, A.K. Mechler, M.T. Sougrati, S. Brüller, K. Strickland, Q. Jia, S. Mukerjee, K.J.J. Mayrhofer, F. Jaouen, *Angew. Chem. Int. Ed.* 56 (2017) 8809.
- [67] J.R. Pels, F. Kapteijn, J.A. Moulijn, Q. Zhu, K.M. Thomas, *Carbon* 33 (1995) 1641.
- [68] M. Ferrandon, A.J. Kropf, D.J. Myers, *J. Phys. Chem. C* 116 (2012) 16001.
- [69] K. Wu, C. Hung, *Appl. Surf. Sci.* 256 (2009) 1595.
- [70] G. Wu, P. Zelenay, *Acc. Chem. Res.* 46 (2013) 1878.
- [71] L. He, F. Weniger, H. Neumann, M. Beller, *Angew. Chem. Int. Ed.* 55 (2016) 12582.
- [72] A. Rahimi, A. Azarpira, H. Kim, J. Ralph, S.S. Stahl, *J. Am. Chem. Soc.* 135 (2013) 6415.
- [73] R. Zhu, B. Wang, M. Cui, J. Deng, X. Li, Y. Ma, Y. Fu, *Green Chem.* 18 (2016) 2029.
- [74] L. Shuai, M.T. Amiri, Y.M. Questell-Santiago, F. Héroguel, Y. Li, H. Kim, R. Meilan, C. Chapple, J. Ralph, J.S. Luterbacher, *Science* 354 (2016) 329.